Accurate Analytical Accelerometer–Magnetometer Axes Alignment Guaranteeing Exact Orthogonality

Paul P. Sotiriadis, *Senior Member, IEEE*, and Konstantinos Papafotis, *Graduate Student Member, IEEE*

***Abstract*— A complete analytical solution to the problem of aligning the sensitivity axes (coordinate frames) of a three-axis accelerometer and a three-axis magnetometer, fixed on the same rigid platform, is introduced. It exploits the magnetic inclination phenomenon to analytically derive the axes alignment rotation matrix and the inclination angle. Starting from a popular formulation of the problem as a constrained optimization one, it introduces a transformation and a parameterization, converting it to an unconstrained one within the special orthogonal group. In contrast to existing methods using the same principle, it guarantees the orthogonality of the axes-alignment rotation matrix and achieves best-of-class accuracy at the same time. It is two orders of magnitude faster than the gradient descent and Newton–Raphson-based methods and about three times faster than state-of-the-art semianalytical approaches achieving the same accuracy. Multiple sets of the sensor data are used to demonstrate the method's accuracy and computational efficiency.**

***Index Terms*— Accelerometer, axes alignment, magnetic inclination, magnetometer, optimization.**

I. Introduction

THE advancement of microelectromechanical (MEM) sensors' technology over the past decades enabled the wide use of inertial and magnetic sensors in commercial devices. Nowadays, inertial and magnetic sensors are key parts of our everyday life as they are embedded in a plethora of devices, such as smartphones, activity trackers, alarm systems, and navigation devices.

Sensors based on MEM technology come with two great advantages; they are of miniature size and of extremely low cost. Their main disadvantage, however, compared to larger and costlier devices, is their large(r) error characteristics, which can be prohibiting for many applications. To this purpose, several works proposed calibration methods to compensate for the most important linear, time-invariant sensors' errors [1]–[9]. While such methods are very effective for single-sensor calibration, most of them do not account for cross-sensor axes alignment.

Manuscript received December 2, 2020; revised April 5, 2021; accepted April 17, 2021. Date of publication May 3, 2021; date of current version May 21, 2021. This work was supported by Greece and the European Union (European Social Fund—ESF) through the Operational Program "Human Resources Development, Education and Lifelong Learning" in the context of the project "Strengthening Human Resources Research Potential via Doctorate Research" under Grant MIS-5000432, implemented by the State Scholarships Foundation (IKY). The Associate Editor coordinating the review process for this article was Dr. Bruno Ando. *(Corresponding author: Konstantinos Papafotis.)*

The authors are with the Department of Electrical and Computer Engineering, National Technical University of Athens, 15780 Athens, Greece (e-mail: k.papafotis@gmail.com).

Digital Object Identifier 10.1109/TIM.2021.3075528

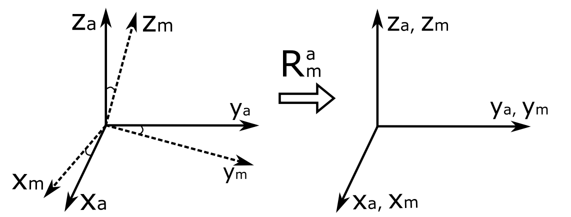

Fig. 1. Axes alignment.

Inertial and magnetic sensors are often used in combination in many applications, including navigation [10] and attitude estimation [11], healthcare systems [12], gaming and entertainment devices [13], space exploration, and many other industrial and commercial ones. In such cases, it is crucial for their sensitivity axes (coordinate frames) to be aligned.

Assuming that the coordinate frames of the accelerometer and the magnetometer are $\{x_a, y_a, z_a\}$ and $\{x_m, y_m, z_m\}$, respectively, aligning the two coordinate frames comes down to deriving a rotation matrix $R_M^A \in \mathrm{SO}(3)$ such that $R_M^A\{x_m, y_m, z_m\} = \{x_a, y_a, z_a\}$, as shown in Fig. 1.

Axes alignment algorithms require an accurately known magnetic field to be used as a reference in order to derive R_M^A. When cost is of no concern, the reference magnetic field is generated using expensive laboratory equipment. For low-cost sensors, however, this is impractical due to incommensurate extra cost.

Several works propose axes alignment methods that require no special piece of equipment [1], [2], [5], [14]–[18]. A standard approach is to exploit the magnetic inclination phenomenon as a reference in order to align the axes of an accelerometer and a magnetometer. Magnetic inclination (or magnetic dip) is the angle between the horizon and the Earth's magnetic field lines, as shown in Fig. 2. It varies with location and time, and the sine of it is the inner product of the normalized gravity and the magnetic field[1] vectors

$$s_\delta \triangleq \sin(\delta) = \frac{g^T m}{\|g\|\|m\|}. \tag{1}$$

Existing axes alignment algorithms, e.g., [1], [2], [15], [17], use (1) and accelerometer's and magnetometer's measurements to form an optimization problem for deriving R_M^A. To do so, some of them [1], [2] form a cost-plus-penalty function

[1] All norms in this article are Euclidean norms, unless stated otherwise

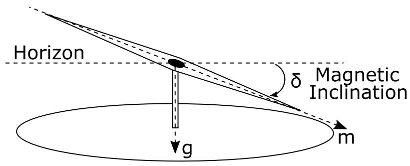

Fig. 2. Magnetic inclination.

associated with (1), which is then minimized using the gradient descent or Newton–Raphson (NR) method.

To ensure that $R_M^A \in \mathrm{SO}(3)$, it is common to include a properly weighted (penalty) term in the cost-plus-penalty function [see (3)]. Selecting the penalty function or its weighting factor is not always trivial. Improper selection can cause the divergence of the derived R_M^A from orthogonality or convergence issues in the gradient descent, NR methods, or other iterative methods.

A closed-form solution for the axes alignment problem is proposed in [19]. While [19] provides a solution such that $R_M^A \in \mathrm{SO}(3)$ (orthogonality and determinant one), it may be less accurate than other solutions derived after many iteration steps of gradient descent and NR methods.

In this work, we propose a complete analytical solution to the axes alignment problem, guaranteeing the orthogonality of the axes alignment rotation matrix, with best-of-class accuracy. This is done by introducing a new formulation of the axes alignment problem that transforms the original constrained optimization problem into a smooth unconstrained one.

The proposed method derives both the magnetic inclination angle and the axes alignment rotation matrix in the closed-form. Due to its analytical nature, the proposed method gives highly accurate results, comparable to the best ones achieved by existing iterative methods, however requiring significantly lower computational resources. Thus, the proposed method is ideal for embedded, low-power devices with limited hardware resources.

The rest of the article is organized as follows. In Section II, the axes alignment problem is analyzed and formulated as an optimization problem. Moreover, the limitations of current works are demonstrated using real sensors' data. In Section III, the proposed method is presented. The evaluation of the proposed method is done in Section IV along with its comparison to other axes alignment methods. Finally, conclusions are drawn in Section V.

II. Problem Statement and Performance Limitations of the Prior Art

Consider a three-axis accelerometer and a three-axis magnetometer, fixed on the same rigid platform. In our analysis, we assume that both sensors have been individually calibrated.

Assume that K accelerometer's measurements $\{g_k\}_{k=1}^K$ and K magnetometer's measurements $\{m_k\}_{k=1}^K$. Each measurement set is naturally expressed in the corresponding sensor's frame, i.e., the $\{A\}$-frame and the $\{M\}$-frame, respectively. Measurements g_k and m_k are taken *simultaneously* when the platform is *still* in $k = 1, 2, \ldots, K$ different orientations and assuming a magnetic field of constant direction[2] in the platform's vicinity.[3] Therefore, $\{g_k\}_{k=1}^K$ are gravity acceleration vectors, and all magnetic field vectors $\{m_k\}_{k=1}^K$ have the same magnitude. Without loss of generality and for convenience purposes, we assume that the vectors are normalized, i.e., $\|g_k\| = \|m_k\| = 1$ for $k = 1, 2, \ldots, K$.

Let R_M^A be the axes alignment matrix, rotating the magnetometer's coordinate $\{M\}$-frame into the accelerometer's $\{A\}$-frame, i.e., $R_M^A m_k$ is the k^{th} magnetic field measurement expressed in the $\{A\}$-frame. For notational convenience, we drop the superscript and the subscript and write $R = R_M^A$.

Then, from (1), we have that $s_\delta = g_k^T R m_k$ for $k = 1, 2, \ldots, K$. Using this, R is commonly calculated by solving the minimization problem [19]

$$\min_{R, s_\delta} \sum_{k=1}^{K} \left(s_\delta - g_k^T R m_k\right)^2 \quad \text{s.t. } R \in \mathrm{SO}(3), \quad |s_\delta| \leq 1. \tag{2}$$

A typical approach to solve (2) is to minimize an associated cost-plus-penalty function using the gradient descent or the NR method. In [1] and [2], the authors use the following cost-plus-penalty function, J_{CP}, associated with (2) and incorporating a weighted penalty term capturing the nonorthogonality of R[4]:

$$J_{\mathrm{CP}}(R, s_\delta) = \sum_{k=1}^{K} \left(s_\delta - g_k^T R m_k\right)^2 + \lambda \|RR^T - I\|_F^2 \tag{3}$$

where $\|\cdot\|_F$ denotes the Frobenius norm. In using (3) in [1] and [2], special care should be given to the selection of the weighting parameter, λ, in order to ensure both the approximate orthogonality of R and the (fast) converge of the minimization method.

Following the iterative optimization approaches [1], [2] and (3), we first consider the case when both R and s_δ are initialized without any prior knowledge, as the identity matrix and zero, respectively. Using the NR method and a set of sensors' measurements, we minimize (3) for multiple values of λ. To assess the distance from orthogonality of the derived matrices R, we first define the nearest orthogonal matrix to R as [20]

$$R_O = UV^T \tag{4}$$

where $U \in O(3)$ and $V \in O(3)$ are defined via a singular value decomposition (SVD) of $R = U\Sigma V^T$. Then, the distance of R from orthogonality is defined as

$$D_O(R) \triangleq \|R - R_O\| = \|R - UV^T\|. \tag{5}$$

The convergence of J_{CP} using the NR for different values of λ is shown in Fig. 3. The numbers of iterations for NR to converge (J_{CP} to drop below 10^{-4}) and the distance of the

[2]The magnitude is irrelevant in the proposed method, and it is normalized.

[3]Typically, in the absence of special calibration equipment, such experiments are conducted under the influence of the Earth's (constant) magnetic field, in an outdoor environment, away from magnetic disturbances, such as buildings and cars [5], [8].

[4]Note that, when the initial condition of the NR is far from the final solution, an extra term in (3) is required to force the determinant of R to be equal to one and thus $R \in \mathrm{SO}(3)$. However, if NR initial condition is near to the final solution, this term may be omitted.

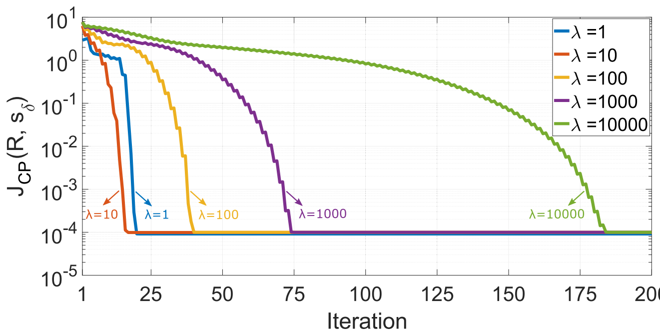

Fig. 3. Convergence of NR for different values of the weighting factor λ (the fastest convergence corresponds to $\lambda = 10$).

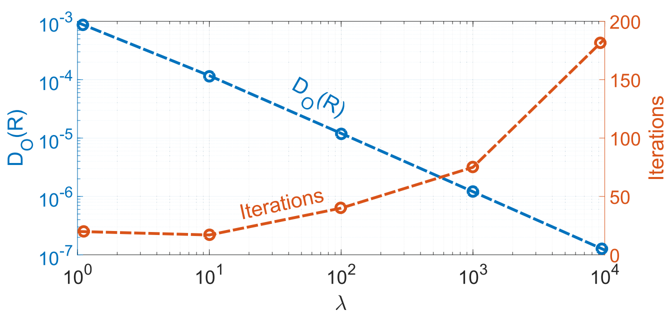

Fig. 4. Distance of R from orthogonality $D_O(R)$ when NR has converged, and the number of iterations required for convergence, as functions of a weighting factor λ.

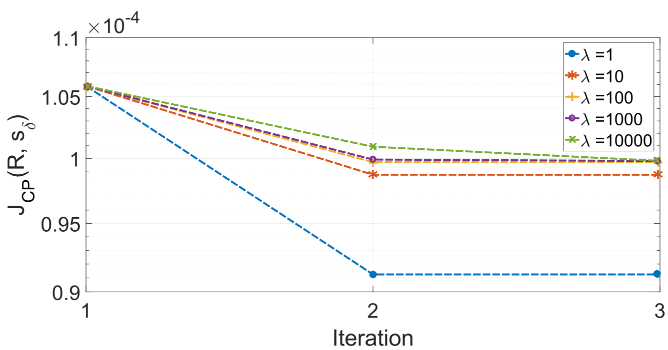

Fig. 5. Convergence of NR for different values of the weighting factor, λ, when the single-step method in [19] is used for initialization.

derived matrix R from orthogonality are presented in Fig. 4 as functions of λ.

We observe that larger values of λ result in R closer to orthogonality. However, NR requires more iterations to converge for larger λ, implying a tradeoff between the orthogonality of R and computational efficiency.

A better tradeoff is obtained when the results of the single-step method in [19] are used to initialize the NR method. As shown in Figs. 5 and 6, NR converges after only two iterations even when large values of λ are used. However, in this case, the computational complexity of the single-step method of [19] must be also taken into account.

III. Proposed Method

The proposed method converts the constrained optimization problem (2) to an unconstrained one, which is solved using

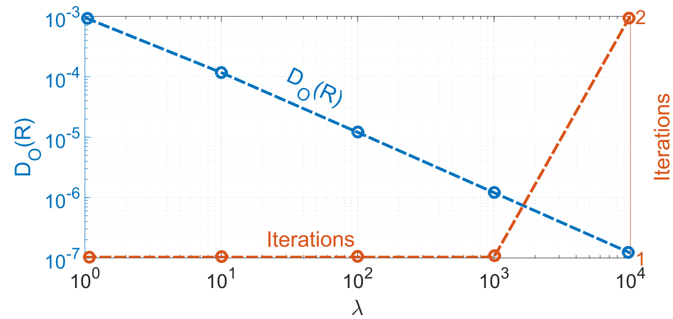

Fig. 6. Distance of R from orthogonality and NR iterations until the convergence for different values of the weighting factor, λ, when the single-step method in [19] is used for initialization.

analytical iterations of the NR method. Furthermore, using a good initial estimate of the point of minimum, as done later in this section, implies that only one iteration is sufficient to achieve a very accurate result.

To convert the constrained problem (2) into an unconstrained one, we first derive the optimal value of s_δ analytically and formulate an equivalent optimization problem with the single unknown R. To do so, consider the cost function of (2)

$$J(R, s_\delta) = \sum_{k=1}^{K} \left(s_\delta - g_k^T R m_k\right)^2 \tag{6}$$

and note that it is quadratic with respect to s_δ. Defining the 9×1 vector $V_R = \mathrm{vec}(R)$ and using the identity $g_k^T R m_k = (m_k \otimes g_k)^T \mathrm{vec}(R)$, we write

$$J(R, s_\delta) = K {s_\delta}^2 - 2 s_\delta \underline{1}^T A V_R + V_R^T A^T A V_R \tag{7}$$

where $\otimes$ is Kronecker's product [21], $\underline{1}$ is the $K \times 1$ vector of ones, and the $K \times 9$ matrix A is

$$A = \begin{bmatrix} (m_1 \otimes g_1)^T \\ (m_2 \otimes g_2)^T \\ \vdots \\ (m_K \otimes g_K)^T \end{bmatrix}. \tag{8}$$

We define the minimum of $J(s_\delta, R)$ with respect to s_δ, that is

$$J_1(R) \triangleq \min_{|s_\delta| \le 1} J(R, s_\delta) \tag{9}$$

and observe that the unconstrained point of minimum is

$$s_\delta^* = \frac{1}{K} \underline{1}^T A V_R. \tag{10}$$

Note that (10) can also be written as

$$s_\delta^* = \frac{1}{K} \sum_{i=1}^{K} \left(g_i^T R m_i\right). \tag{11}$$

Following our assumption that $\|g_i\| = \|m_i\| = 1$ for all $i = 1, 2, \ldots, K$ and the fact that the $\|\cdot\|_2$-norm is rotational invariant, by applying the Cauchy–Schwarz inequality to (11), we get $|s_\delta^*| \le 1$, and so s_δ^* is feasible, and the global minimum of (9).

Replacing (10) into (7), $J_1(R)$ is conveniently written as

$$J_1(R) = \frac{1}{2} V_R^T B V_R \tag{12}$$

where $B = 2(A^T A - (1/K) A^T \underline{1}\ \underline{1}^T A)$ is a 9×9 symmetric matrix. Note that, by the definition of J_1, we have

$$\min_{R \in \mathrm{SO}(3), |s_\delta| \leq 1} J(R, s_\delta) = \min_{R \in \mathrm{SO}(3)} J_1(R) \tag{13}$$

where the minimum exists since the cost function J_1 is continuous and SO(3) is compact.

Let $R_* \in \mathrm{SO}(3)$ be a point of global minimum of J_1 that is

$$J_1(R_*) = \min_{R \in \mathrm{SO}(3)} J_1(R) \tag{14}$$

and let $R_0 \in \mathrm{SO}(3)$ be an initial estimate of R_*. An improved estimate can always be expressed as $R = P R_0$, for some $P \in \mathrm{SO}(3)$. Moreover, we can write P as a sequence of three Euler rotations, that is

$$P = P(x) \triangleq R_z(\phi) R_y(\psi) R_x(\theta) \tag{15}$$

where ϕ, ψ, and θ are the yaw, pitch, and roll rotation angles, respectively, $x \triangleq [\phi,\ \psi,\ \theta]^T$, and

$$R_z(\phi) = \begin{bmatrix} \cos(\phi) & -\sin(\phi) & 0 \\ \sin(\phi) & \cos(\phi) & 0 \\ 0 & 0 & 1 \end{bmatrix}$$
$$R_y(\psi) = \begin{bmatrix} \cos(\psi) & 0 & -\sin(\psi) \\ 0 & 1 & 0 \\ \sin(\psi) & 0 & \cos(\psi) \end{bmatrix}$$
$$R_x(\theta) = \begin{bmatrix} 1 & 0 & 0 \\ 0 & \cos(\theta) & -\sin(\theta) \\ 0 & \sin(\theta) & \cos(\theta) \end{bmatrix}. \tag{16}$$

The function $P : [0, 2\pi)^3 \rightarrow SO(3)$ is surjective and so $R = P(x) R_0$ can take any matrix value in SO(3), [22].

The above converts the original optimization problem to the one of deriving x such that $P(x) R_0 = R_*$. To proceed further, it is convenient to define the cost as a function of x, that is

$$J_2(x) \triangleq J_1(P(x) R_0) = \frac{1}{2} V_R(x)^T B V_R(x) \tag{17}$$

where $V_R(x) = \mathrm{vec}(R(x)) = \mathrm{vec}(P(x) R_0)$.

Assume that R_0 and $R = P R_0$ are close to R_*, i.e., $\|R_0 - R_*\|_F$ and $\|R - R_*\|_F$ are small.[5] Then, P is close to the identity matrix, and so there exists a small x such that $P = P(x)$, [22]. This along with the smoothness of the functions involved motivates the use of minimization methods based on the Taylor expansion, such as NR.

To minimize $J_2(x)$, we have to derive x such that $\partial J_2 / \partial x = 0$. To do so, we start from $x = 0$, implying $P(x) = I$ and cost $J_2(0)$, apply one iteration (or more) of NR method, and derive the new value of x as

$$x = -\left(\left. \frac{\partial^2 J_2}{\partial x \partial x^T} \right|_{x=0} \right)^{-1} \left. \frac{\partial J_2}{\partial x} \right|_{x=0}. \tag{18}$$

The cost gradient is

$$\frac{\partial J_2}{\partial x} = \left[\frac{\partial J_2}{\partial \phi},\ \frac{\partial J_2}{\partial \psi},\ \frac{\partial J_2}{\partial \theta} \right]^T \tag{19}$$

[5]With respect to the Frobenius or any other rotational invariant matrix norm.

and the Hessian matrix is symmetric and written as

$$\frac{\partial^2 J_2}{\partial x \partial x^T} = \begin{bmatrix} \frac{\partial^2 J_2}{\partial \phi^2} & \frac{\partial^2 J_2}{\partial \phi \partial \psi} & \frac{\partial^2 J_2}{\partial \phi \partial \theta} \\ \frac{\partial^2 J_2}{\partial \phi \partial \psi} & \frac{\partial^2 J_2}{\partial \psi^2} & \frac{\partial^2 J_2}{\partial \psi \partial \theta} \\ \frac{\partial^2 J_2}{\partial \phi \partial \theta} & \frac{\partial^2 J_2}{\partial \psi \partial \theta} & \frac{\partial^2 J_2}{\partial \theta^2} \end{bmatrix} \tag{20}$$

because of the continuity of all second derivatives.

We derive the first and second derivatives at $x = 0$, analytically recalling that $B^T = B$. From (17) and for s, $q \in \{\phi, \psi, \theta\}$, we have that

$$\frac{\partial J_2}{\partial q} = V_R^T B \frac{\partial V_R}{\partial q} \tag{21}$$

and

$$\frac{\partial^2 J_2}{\partial s \partial q} = \frac{\partial V_R^T}{\partial s} B \frac{\partial V_R}{\partial q} + V_R^T B \frac{\partial^2 V_R}{\partial s \partial q}. \tag{22}$$

From the definition $V_R = \mathrm{vec}(R)$, we have that

$$\frac{\partial V_R}{\partial q} = \mathrm{vec}\left(\frac{\partial R}{\partial q} \right) \tag{23}$$

and

$$\frac{\partial^2 V_R}{\partial s \partial q} = \mathrm{vec}\left(\frac{\partial^2 R}{\partial s \partial q} \right). \tag{24}$$

Moreover, since $R(x) = P(x) R_0 = R_z(\phi) R_y(\psi) R_x(\theta) R_0$, from (16), it is

$$\left. \frac{\partial R}{\partial q} \right|_{x=0} = P_q R_0 \tag{25}$$

for $q \in \{\phi, \psi, \theta\}$, and

$$\left. \frac{\partial^2 R}{\partial s \partial q} \right|_{x=0} = P_s P_q R_0 \tag{26}$$

for the ordered pairs

$$(s, q) \in \{(\phi, \phi), (\phi, \psi), (\phi, \theta), (\psi, \psi), (\psi, \theta), (\theta, \theta)\} \tag{27}$$

where

$$P_\phi = \begin{bmatrix} 0 & -1 & 0 \\ 1 & 0 & 0 \\ 0 & 0 & 0 \end{bmatrix}$$
$$P_\psi = \begin{bmatrix} 0 & 0 & -1 \\ 0 & 0 & 0 \\ 1 & 0 & 0 \end{bmatrix}$$
$$P_\theta = \begin{bmatrix} 0 & 0 & 0 \\ 0 & 0 & -1 \\ 0 & 1 & 0 \end{bmatrix}. \tag{28}$$

Combining (23) with (25) and (24) with (26), respectively, gives

$$\left. \frac{\partial V_R}{\partial q} \right|_{x=0} = (I_3 \otimes P_q) V_{R_0} \tag{29}$$

and

$$\left. \frac{\partial^2 V_R}{\partial s \partial q} \right|_{x=0} = \big(I_3 \otimes (P_s P_q)\big) V_{R_0} \tag{30}$$

where $V_{R_0} = \text{vec}(R_0)$. Finally, replacing (29) into (21) gives

$$\left.\frac{\partial J_2}{\partial q}\right|_{x=0} = V_{R_0}^T B(I_3 \otimes P_q) V_{R_0}. \tag{31}$$

Similarly, replacing (29) and (30) into (22) gives

$$\left.\frac{\partial^2 J_2}{\partial s \partial q}\right|_{x=0} = V_{R_0}^T (I_3 \otimes P_s^T) B(I_3 \otimes P_q) V_{R_0} + V_{R_0}^T B\big(I_3 \otimes (P_s P_q)\big) V_{R_0}. \tag{32}$$

Note that (32) is valid (only) for the six (s, q) pairs in (27).

The proper selection of the initial matrix R_0 is crucial for achieving (fast) convergence. To this purpose, we recommend using as R_0 the approximate closed-form solution of (2) derived in [19]. This is done as follows. Using A defined in (8), we calculate the 9×1 vector $(A^T A)^{-1} A^T \underline{1}$ and split it into three 3×1 vectors h_1, h_2, and h_3, that is

$$(A^T A)^{-1} A^T \underline{1} = \begin{bmatrix} h_1^T & h_2^T & h_3^T \end{bmatrix}^T. \tag{33}$$

Then, using h_1, h_2, and h_3, we form the matrix

$$H = \begin{bmatrix} h_1 & h_2 & h_3 \end{bmatrix}. \tag{34}$$

We consider an SVD of matrix H, i.e., $H = U \Sigma V^T$, where $U, V \in O(3)$ and Σ is the diagonal matrix $\Sigma = \text{diag}(\sigma_1, \sigma_2, \sigma_3)$, with $\sigma_1 \geq \sigma_2 \geq \sigma_3 > 0$, assuming that $\text{rank}(A) = 9$. The approximation $R_0 \in SO(3)$ of the axes rotation matrix R_* is given by

$$R_0 = \text{sgn}(\det(H)) U V^T. \tag{35}$$

For more information about the derivation of (35), the reader is referred to [19].

The complete proposed method using only one analytical iteration of the NR (which is typically sufficient) is summarized in Algorithm 1.

Algorithm 1 Proposed Method

1: Use normalized g_k and m_k to form matrix A in (8)
2: Verify that A is of full rank
3: Use (33), (34) and (35) to calculate R_0 as in [19]
4: Calculate the gradient vector using (19) and (31)
5: Calculate the Hessian matrix using (20) and (32)
6: Calculate x from (18)
7: Use x to calculate $P(x)$ using (15) and (16)
8: Calculate $R = P(x) R_0 \in SO(3)$.

IV. Evaluation of the Proposed Method

Let $R_M^A \in SO(3)$ be the frame transformation matrix rotating the magnetometer's coordinate frame into the accelerometer's one. To evaluate the accuracy and computational efficiency of the proposed method, we have to compare the derived axes alignment matrix, R, to the actual one, R_M^A, which we assume to know accurately in advance.

However, the accuracy with which one can measure R_M^A using laboratory equipment is orders of magnitude worse than the expected accuracy of the proposed method. Therefore, we artificially generated 1000 datasets with preselected $R_M^A \in \text{SO}(3)$, according to the calibration procedure introduced in [1]. This included the random errors (noise) of the sensors and the associated instrumentation according to typical characteristics of commercial devices.

TABLE I

Mean Value and Variance of the Error ε of the Proposed Method, a Gradient Descent (GD)-Based Method, an NR-Based Method, an NR-Based Method Initialized Using the Solution of [19], and the Single-Step Method of [19] Alone

Method	$\boldsymbol{\mu_\varepsilon}$	$\boldsymbol{\sigma_\varepsilon^2}$	**Time (ms)**
GD	$7.16 \cdot 10^{-4}$	$9.90 \cdot 10^{-8}$	63.15
NR	$7.17 \cdot 10^{-4}$	$9.95 \cdot 10^{-8}$	44.53
NR & [20]	$7.15 \cdot 10^{-4}$	$9.92 \cdot 10^{-8}$	1.34
Single-Step [20]	$11.60 \cdot 10^{-4}$	$56.53 \cdot 10^{-8}$	0.25
Proposed	$7.14 \cdot 10^{-4}$	$9.94 \cdot 10^{-8}$	0.49

To generate the 1000 datasets, we first randomly generated 1000 values of $R_A^M = (R_M^A)^T \in \text{SO}(3)$. For every one of them, we have followed the following steps.

1) First, we generated two random unit vectors, g_1^A and m_1^A, representing the gravity and the magnetic field in the accelerometer's $\{A\}$-frame.
2) We rotated both vectors 11 times according to [1] to generate $\{g_i^A\}_{i=2}^{12}$ and $\{m_i^A\}_{i=2}^{12}$.
3) To express the magnetic field vectors $\{m_i^A\}_{i=1}^{12}$ in the magnetometer's $\{M\}$-frame, we rotated them once more using R_A^M to get $\{m_i^M\}_{i=1}^{12}$
4) Finally, a sequence of band-limited white noise was added to the dataset following typical sensors' and measuring procedure's specifications.

We compare our method's accuracy and execution time to those of: 1) a gradient descent based method using (3); 2) an NR-based method using (3); 3) an NR-based method using (3), initialized using the solution of the single-step method presented in [19]; and 4) the single-step method of [19] alone.

Each of the aforementioned methods was run for every one of the 1000 generated datasets. For the iterative methods, based on the gradient descent and the NR, the parameter λ of the cost function (3) was set to $\lambda = 1000$ to ensure the orthogonality of the derived matrix R according to Figs. 4 and 6. We compared the derived matrix R, of each method, with the true rotation matrix $R_M^A = (R_A^M)^T$ used to generate the data. To quantify their difference, we used the error metric

$$\varepsilon = \left\| R - R_M^A \right\|. \tag{36}$$

In the ideal case of perfect axes alignment, i.e., $R = R_M^A$, it is $\varepsilon = 0$. The mean value (μ_ε) and variance (σ_ε^2) of ε for every method are presented in Table I.

As shown in Table I, the gradient descent and the NR-based methods alone yield accurate results, however requiring significant computational effort. The single-step method of [19] has much better computational efficiency, but it is a little less accurate. The proposed method excels in both accuracy and computational efficiency. It provides accurate results, similar to those of the computationally heavy, iterative optimization

TABLE II

PERFORMANCE CHARACTERISTICS OF THE ACCELEROMETER (A) AND THE MAGNETOMETER (M) INCLUDED IN THE DESIGNED MEASUREMENT DEVICE

Specification	**Value**
Measurement Range (A)	$\pm 16g$
Measurement Range (M)	$\pm 4Gauss$
Sampling Rate (A)	$238Hz$
Sampling Rate (M)	$80Hz$
Resolution (A, M)	$16Bits$

TABLE III

RESIDUAL ERROR OF THE PROPOSED METHOD, A GRADIENT DESCENT (GD)-BASED METHOD, AN NR-BASED METHOD, AN NR-BASED METHOD INITIALIZED USING THE SOLUTION OF [19], AND THE "SINGLE-STEP" METHOD OF [19] EVALUATED USING FIVE DIFFERENT DATASETS (D1–D5) OF REAL SENSORS' DATA

	$J_{CP}(R, s_\delta) \cdot 10^4$				
Method	**D1**	**D2**	**D3**	**D4**	**D5**
GD	7.02	7.33	7.12	6.40	7.49
NR	7.02	7.35	7.24	6.38	7.37
NR & [20]	7.01	7.32	7.16	6.39	7.53
Single-Step [20]	9.36	9.21	9.12	8.42	9.68
Proposed	7.01	7.33	7.09	6.37	7.72

methods, while it requires significantly less computational resources.

While artificially generated data are appropriate to evaluate the accuracy and computational efficiency of the proposed algorithm, they do not incorporate the nonidealities expected in real-world measurements. Although we included random noise in the artificially generated data, other errors, such as residual calibration errors (of the sensors individually), could degrade the proposed algorithm's performance.

To demonstrate the resilience of the proposed algorithm to such effects, we recorded five different datasets of accelerometer's and magnetometer's measurements. To this end, we used a measurement device based on the LSM9DS1 system-in-package by STMicroelectronics, which includes both a three-axis accelerometer and a three-axis magnetometer. Some important performance characteristics of the two sensors and the developed measurement device are presented in Table II.

All datasets were recorded away from magnetic disturbances (the constant earth's magnetic field was used as reference) following the calibration procedure introduced in [1]. Specifically, to record each dataset, we placed the measurement device by hand in 12 different orientations, as suggested in [1]. In each orientation, we recorded several measurements, while the sensor was still and used averaging to obtain 12 pairs of accelerometer's and magnetometer's measurements corresponding to the 12 orientations.

In this case of real sensors' data, the true matrix R_M^A is not known. Thus, in order to evaluate the accuracy of the proposed algorithm and compare it to that of the existing ones, we use the cost-plus-penalty function of (3) as a metric of the residual error.

In Table III, we used five different datasets (D1–D5) to compare our method's residual error to that of: 1) a gradient descent based method using (3); 2) an NR-based method using (3); 3) an NR-based method using (3), initialized using the solution of the single-step method presented in [19]; and 4) the single-step method of [19].

Again, for the iterative methods, based on the gradient descent and the NR, the parameter λ of the cost function (3) was set to $\lambda = 1000$, to ensure the orthogonality of the derived matrix R according to Figs. 4 and 6.

V. CONCLUSION

This work introduced an analytical method for aligning the axes of a three-axis accelerometer and a three-axis magnetometer. The method guarantees the orthogonality of the axes-alignment rotation matrix and achieves best-of-class accuracy, while it excels in computational efficiency by being two orders of magnitude faster than existing methods of the same accuracy. Moreover, it does not require any parametrization in contrast to optimization-based methods depending on proper parametrization to converge to feasible solutions. The advantages of the proposed method source from the different formulation of the axes alignment optimization problem introduced.

REFERENCES

[1] K. Papafotis and P. P. Sotiriadis, "MAG.I.C.AL.—A unified methodology for magnetic and inertial sensors calibration and alignment," *IEEE Sensors J.*, vol. 19, no. 18, pp. 8241–8251, Sep. 2019.

[2] K. Papafotis and P. P. Sotiriadis, "Accelerometer and magnetometer joint calibration and axes alignment," *Technologies*, vol. 8, no. 1, p. 11, Jan. 2020.

[3] R. Alonso and M. D. Shuster, "TWOSTEP: A fast robust algorithm for attitude-independent magnetometer-bias determination," *J. Astron. Sci.*, vol. 50, no. 4, pp. 433–451, Dec. 2002.

[4] Y. Wu and W. Shi, "On calibration of three-axis magnetometer," *IEEE Sensors J.*, vol. 15, no. 11, pp. 6424–6431, Nov. 2015.

[5] M. Kok and T. B. Schön, "Maximum likelihood calibration of a magnetometer using inertial sensors," *IFAC Proc. Volumes*, vol. 47, no. 3, pp. 92–97, 2014.

[6] J. F. Vasconcelos, G. Elkaim, C. Silvestre, P. Oliveira, and B. Cardeira, "Geometric approach to strapdown magnetometer calibration in sensor frame," *IEEE Trans. Aerosp. Electron. Syst.*, vol. 47, no. 2, pp. 1293–1306, Apr. 2011.

[7] X. Lu, Z. Liu, and J. He, "Maximum likelihood approach for low-cost MEMS triaxial accelerometer calibration," in *Proc. 8th Int. Conf. Intell. Hum.-Mach. Syst. Cybern. (IHMSC)*, Aug. 2016, pp. 179–182.

[8] N. Ammann, A. Derksen, and C. Heck, "A novel magnetometer-accelerometer calibration based on a least squares approach," in *Proc. Int. Conf. Unmanned Aircr. Syst. (ICUAS)*, Jun. 2015, pp. 577–585.

[9] Y. Zhong, Y. Xu, N. He, and X. Yu, "A new drone accelerometer calibration method," in *Proc. 37th Chin. Control Conf. (CCC)*, Jul. 2018, pp. 9928–9933.

[10] C. Fischer, P. T. Sukumar, and M. Hazas, "Tutorial: Implementing a pedestrian tracker using inertial sensors," *IEEE Pervas. Comput.*, vol. 12, no. 2, pp. 17–27, Apr. 2013.

[11] S. O. H. Madgwick, A. J. L. Harrison, and R. Vaidyanathan, "Estimation of IMU and MARG orientation using a gradient descent algorithm," in *Proc. IEEE Int. Conf. Rehabil. Robot.*, Jun. 2011, pp. 1–7.

[12] T. Shi, X. Sun, Z. Xia, L. Chen, and J. Liu, "Fall detection algorithm based on triaxial accelerometer and magnetometer," *Eng. Lett.*, vol. 24, no. 2, pp. 157–167, 2016.

[13] C.-H. Chu, "Video stabilization for stereoscopic 3D on 3D mobile devices," in *Proc. IEEE Int. Conf. Multimedia Expo (ICME)*, Jul. 2014, pp. 1–6.

[14] Y. Wu, D. Zou, P. Liu, and W. Yu, "Dynamic magnetometer calibration and alignment to inertial sensors by Kalman filtering," *IEEE Trans. Control Syst. Technol.*, vol. 26, no. 2, pp. 716–723, Mar. 2018.

[15] M. Kok, J. D. Hol, T. B. Schön, F. Gustafsson, and H. Luinge, "Calibration of a magnetometer in combination with inertial sensors," in *Proc. 15th Int. Conf. Inf. Fusion*, Singapore, Jul. 2012, pp. 787–793.

[16] J. Metge, R. Mégret, A. Giremus, Y. Berthoumieu, and T. Décamps, "Calibration of an inertial-magnetic measurement unit without external equipment, in the presence of dynamic magnetic disturbances," *Meas. Sci. Technol.*, vol. 25, no. 12, Dec. 2014, Art. no. 125106. [Online]. Available: http://stacks.iop.org/0957-0233/25/i=12/a=125106

[17] M. V. Gheorghe, "Calibration for tilt-compensated electronic compasses with alignment between the magnetometer and accelerometer sensor reference frames," in *Proc. IEEE Int. Instrum. Meas. Technol. Conf. (I2MTC)*, May 2017, pp. 1–6.

[18] X. Li and Z. Li, "A new calibration method for tri-axial field sensors in strap-down navigation systems," *Meas. Sci. Technol.*, vol. 23, no. 10, Sep. 2012, Art. no. 105105.

[19] P. P. Sotiriadis and K. Papafotis, "A single-step method for accelerometer and magnetometer axes alignment," *IEEE Trans. Instrum. Meas.*, vol. 70, pp. 1–7, 2021.

[20] P. H. Schönemann, "A generalized solution of the orthogonal procrustes problem," *Psychometrika*, vol. 31, no. 1, pp. 1–10, Mar. 1966.

[21] R. A. Horn and C. R. Johnson, *Matrix Analysis*. Cambridge, U.K.: Cambridge Univ. Press, 2013.

[22] P. D. Groves, *Principles of GNSS, Inertial, and Multisensor Integrated Navigation Systems*. Norwood, MA, USA: Artech House, 2013.

Paul P. Sotiriadis (Senior Member, IEEE) received the diploma degree in electrical and computer engineering from the Department of Electrical and Computer Engineering, National Technical University of Athens, Athens, Greece, in 1994, the M.S. degree in electrical engineering from Stanford University, Stanford, CA, USA, in 1996, and the Ph.D. degree in electrical engineering and computer science from the Massachusetts Institute of Technology, Cambridge, MA, USA, in 2002.

In 2002, he joined the Johns Hopkins University, Baltimore, MD, USA, as an Assistant Professor of electrical and computer engineering. In 2012, he joined the Faculty of the Electrical and Computer Engineering Department, National Technical University of Athens. He is a Faculty Member of the Electrical and Computer Engineering Department, National Technical University of Athens, the Director of the Electronics Laboratory of the university, and a member of the Governing Board of the Hellenic Space Center, Chalandri, Greece, and the National Space Center of Greece, Chalandri. He has authored or coauthored more than 150 research publications, most of them in IEEE journals and conferences, and contributed chapters to technical books. He holds one patent. He has led several projects in these fields funded by U.S. Organizations and has collaborations with Industry and National Laboratories. His research interests include design, optimization, and mathematical modeling of analog and mixed-signal circuits, RF and microwave circuits, advanced frequency synthesis, biomedical instrumentation, and interconnect networks in deep-submicrometer technologies.

Dr. Sotiriadis was a member of technical committees of many conferences. He was a recipient of the Best Paper Award in the IEEE International Symposium on Circuits and Systems in 2007, the Guillemin-Cauer Award from the IEEE Circuits and Systems Society in 2012, the Best Paper Award in the IEEE International Frequency Control Symposium in 2012, and the Best Paper Award in the IEEE International Conference on Modern Circuits and Systems Technologies in 2019. He is an Associate Editor of the IEEE SENSORS JOURNAL. He served as an Associate Editor for the IEEE TRANSACTIONS ON CIRCUITS AND SYSTEMS II: EXPRESS BRIEFS from 2005 to 2010 and the IEEE TRANSACTIONS ON CIRCUITS AND SYSTEMS I: REGULAR PAPERS from 2016 to 2020. He regularly reviews for many IEEE Transactions and Conferences and serves on proposal review panels.

Konstantinos Papafotis (Graduate Student Member, IEEE) received the diploma degree in electrical and computer engineering from the National Technical University of Athens, Athens, Greece, in 2015. He is currently pursuing the Ph.D. degree with the Department of Electrical and Computer Engineering, National Technical University of Athens, under the supervision of Prof. Paul P. Sotiriadis.

He is a teaching assistant in several undergraduate courses and acts as an advisor for several diploma theses. He has authored or coauthored several conference papers and journal articles. His main research interests include inertial navigation, embedded systems, and wireless sensor systems.

Dr. Papafotis was a recipient of the Best Paper Award in the IEEE International Conference on Modern Circuits and Systems Technologies in 2019. He is a regular reviewer for many IEEE publications.